Butane Dry Reforming Catalyzed by Cobalt Oxide Supported on Ti_2AlC MAX Phase

Maria Ronda-Lloret,[a] Vijaykumar S. Marakatti,[b] Willem G. Sloof,[c] Juan José Delgado,[d] Antonio Sepúlveda-Escribano,[e] Enrique V. Ramos-Fernandez,[e] Gadi Rothenberg,[a] and N. Raveendran Shiju*[a]

MAX ($M_{n+1}AX_n$) phases are layered carbides or nitrides with a high thermal and mechanical bulk stability. Recently, it was shown that their surface structure can be modified to form a thin non-stoichiometric oxide layer, which can catalyze the oxidative dehydrogenation of butane. Here, the use of a Ti_2AlC MAX phase as a support for cobalt oxide was explored for the dry reforming of butane with CO_2, comparing this new catalyst to more traditional materials. The catalyst was active and selective to synthesis gas. Although the surface structure changed during the reaction, the activity remained stable. Under the same conditions, a titania-supported cobalt oxide catalyst gave low activity and stability due to the agglomeration of cobalt oxide particles. The Co_3O_4/Al_2O_3 catalyst was active, but the acidic surface led to a faster deactivation. The less acidic surface of the Ti_2AlC was better at inhibiting coke formation. Thanks to their thermal stability and acid-base properties, MAX phases are promising supports for CO_2 conversion reactions.

Introduction

The increase in anthropogenic CO_2 emissions and its contribution to the rising average global temperatures makes CO_2 capture and utilization a priority research area.[1–4] Catalytic dry reforming of lower alkanes to CO and H_2 is an interesting option, because the syngas product can be used as feedstock to obtain high-value chemicals through processes such as the Fischer-Tropsch synthesis.[5–8] However, as with any chemical process that uses CO_2, this reaction must overcome a high thermodynamic barrier, which usually means high reaction temperatures. Butane, which is a side product of crude oil cracking and is widely available from shale gas,[9] is thermodynamically less stable ($\Delta G^0_{(n\text{-}C_4H_{10})} = -16.6\ kJ\cdot mol^{-1}$) than smaller hydrocarbons such as methane ($\Delta G^0_{(CH_4)} = -50.5\ kJ\cdot mol^{-1}$). Therefore, dry reforming of butane (DRB) allows us to bring down the reaction temperature to 500–600 °C.[10–13] The problem is that dry reforming catalysts usually suffer from deactivation through sintering of active sites and coking.[14] Even if we can lower the reaction temperature by using butane, catalyst deactivation by coking will still occur by the Boudouard reaction ($2CO \rightarrow CO_2 + C$) and/or via the partial or total cracking of butane.

Traditionally, such reactions use catalysts containing alumina, silica, or titania as supports.[15] Most of the attention is typically focused on the active site. Yet the support plays a crucial role in real-life catalysis, as deactivation via coking and/or strong metal–support interaction (SMSI) preclude the industrial use of many catalysts that show good short-term activity.[16] To address this problem, we turned to a new family of support materials: MAX phases ($M_{n+1}AX_n$). MAX phases are ternary carbides or nitrides with layered hexagonal crystal structures (Figure 1).[17] Their name reflects their chemical composition: M is an early transition metal, A is an A-group element (mostly from groups 13 and 14), X is carbon and/or nitrogen, and $n = 1$, 2, or 3. MAX phases combine an unusual set of thermal, mechanical, and electrical properties. Like ceramics, they show high-temperature strength and stiffness, and at the same time they are tough, ductile, and conduct electricity and heat like metals.[18,19]

Due to their thermal stability and resistance to fracturing, MAX phases have mainly been used for mechanical and thermal

[a] M. Ronda-Lloret, Dr. G. Rothenberg, Dr. N. R. Shiju
Van 't Hoff Institute for Molecular Sciences
University of Amsterdam
Science Park 904, 1090GD Amsterdam (The Netherlands)
E-mail: n.r.shiju@uva.nl
[b] Dr. V. S. Marakatti
Institute of Condensed Matter and Nanosciences (IMCN), Molecular Chemistry, Materials and Catalysis (MOST)
Université Catholique de Louvain (UCLouvain)
Place Louis Pasteur 1, L4.01.09, 1348 Louvain-la-Neuve (Belgium)
[c] Dr. W. G. Sloof
Department of Materials Science and Engineering
Delft University of Technology
Mekelweg 2, 2628 CD Delft (The Netherlands)
[d] Dr. J. J. Delgado
Departamento de Ciencia de los Materiales e Ingeniería Metalúrgica y Química Inorgánica
University of Cádiz
Apdo. 40 Puerto Real, 11510 Cádiz (Spain)
[e] Prof. Dr. A. Sepúlveda-Escribano, Dr. E. V. Ramos-Fernandez
Laboratorio de Materiales Avanzados, Departamento de Química Inorgánica–Instituto, Universitario de Materiales de Alicante, Universidad de Alicante
Apartado 99, 03080 Alicante (Spain)

Supporting information for this article is available on the WWW under https://doi.org/10.1002/cssc.202001633

This publication is part of a Special Issue entitled "Green Carbon Science: CO_2 Capture and Conversion". Please visit the issue at http://doi.org/10.1002/cssc.v13.23.

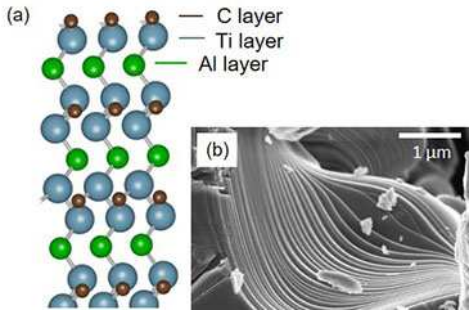

Figure 1. a) Hexagonal crystal structure of Ti_2AlC MAX phase. This material has one Al layer for every second layer of Ti. b) Scanning electron microscopy (SEM) image of Ti_2AlC, showing its layered structure.

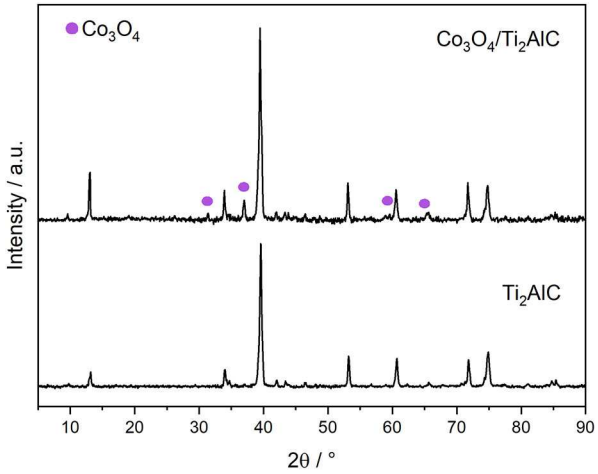

Figure 2. XRD patterns of Co_3O_4/Ti_2AlC catalyst and the Ti_2AlC MAX phase used as support.

applications,[20,21] such as structural coatings in fission and fusion reactors.[22,23] Recently, we showed that MAX phases also have interesting catalytic properties. Though a carbide, Ti_3AlC_2 MAX phase catalyzed butane oxidative dehydrogenation (ODH) with a higher selectivity than common oxide materials. The non-stoichiometric oxide surface layer containing oxygen vacancies made this material catalytically active.[24]

Here, we employ a different approach, using the MAX phases as catalyst supports. Specifically, we were interested in realizing the yet unexplored potential of MAX phases as highly stable and crystalline carbides for developing active dry reforming catalysts that are both stable and coke-resistant. We chose Ti_2AlC, one of the most accessible and most stable MAX phases, as support for cobalt oxide, using this as a catalyst for dry reforming of butane.

Results and Discussion

Catalyst synthesis

Opting for Ti_2AlC as one of the most stable MAX phases, we prepared and tested Co_3O_4/Ti_2AlC as a catalyst for dry reforming of butane, and compared it to two benchmarks, Co_3O_4/Al_2O_3 and Co_3O_4/TiO_2. The catalyst samples, each containing 5 wt% of metallic cobalt, were prepared by wet impregnation, using $Co(NO_3)_2 \cdot 6H_2O$ as the cobalt precursor. The Ti_2AlC support was prepared by mixing Ti, Al, and TiC powders at 1350 °C and high pressure, following the procedure of Boatemaa et al.[18] Anatase titania and γ-Al_2O_3 supports were purchased from commercial sources. We also compared the MAX phase support to commercial α-Al_2O_3 and TiC supports. After impregnation, all catalysts were dried at 120 °C for 2 h, and then calcined in air at 450 °C for 4 h (see the Experimental Section for detailed procedures).

Catalyst characterization

The X-ray diffraction (XRD) pattern of the as-prepared Co_3O_4/Ti_2AlC catalyst (Figure 2) shows the characteristic peaks of the Ti_2AlC MAX phase structure. It also shows the presence of Co_3O_4 at $2\theta = 31.4$, 36.9, 59.5, and 65.6°. Conversely, the Co_3O_4 characteristic peaks are absent from the patterns of Co_3O_4/TiO_2 and Co_3O_4/Al_2O_3 (see Figure S1). Co_3O_4 and $CoAl_2O_4$ both have a spinel structure with almost identical diffraction patterns, which are also similar to those of the γ-Al_2O_3 support. These peaks are visible in the diffraction pattern of the Co_3O_4/Al_2O_3 catalyst at $2\theta = 31.5$, 37.0, 45.7, and 59.4°.[25,26] The pattern of Co_3O_4/TiO_2 only shows the characteristic peaks of TiO_2 anatase, indicating that the Co_3O_4 particles are smaller when supported on TiO_2 compared to Ti_2AlC or Al_2O_3.[27] Scanning transmission electron microscopy (STEM) combined with high-angle annular dark field (HAADF) imaging of Co_3O_4/Ti_2AlC (Figure 3) showed significant agglomeration of cobalt oxide particles, between 90–500 nm in diameter. These particles are hollow, with very small voids. TEM images gave a better insight into the distribution of the hollow structure. The voids are typically 6–30 nm in diameter. These voids result from the Kirkendall effect, where the diffusion rates of the cations and anions differ during oxidation.[28,29] Using Al_2O_3 as a support gives smaller cobalt oxide particles compared to Ti_2AlC, but they also form agglomerates on the support (Figure S2a). The Co_3O_4/TiO_2 catalyst shows the best Co_3O_4 dispersion (Figure S2b). Similar Co_3O_4 hollow structures were reported by Wang et al., following $CoCl_2$ impregnation-reduction-oxidation treatment on a carbon support.[30]

The low surface area of the Ti_2AlC support (typically $< 40\ m^2 \cdot g^{-1}$) explains the low surface area of Co_3O_4/Ti_2AlC, as well as the low dispersion and the large Co_3O_4 particle size.[31] Co_3O_4/Al_2O_3 and Co_3O_4/TiO_2 catalysts are mesoporous materials with a Brunauer–Emmett-Teller (BET) surface area of 187 and $76\ m^2 \cdot g^{-1}$, respectively (see Figure S3 and Table S1 in the Supporting Information for details).

We then studied the reducibility of Co_3O_4 particles and their interaction with the different supports by hydrogen temperature-programmed reduction (TPR) (Figure S4). The reduction of Co_3O_4 particles to CoO is known to occur at lower temperatures. Thereafter, CoO is reduced to metallic Co at higher

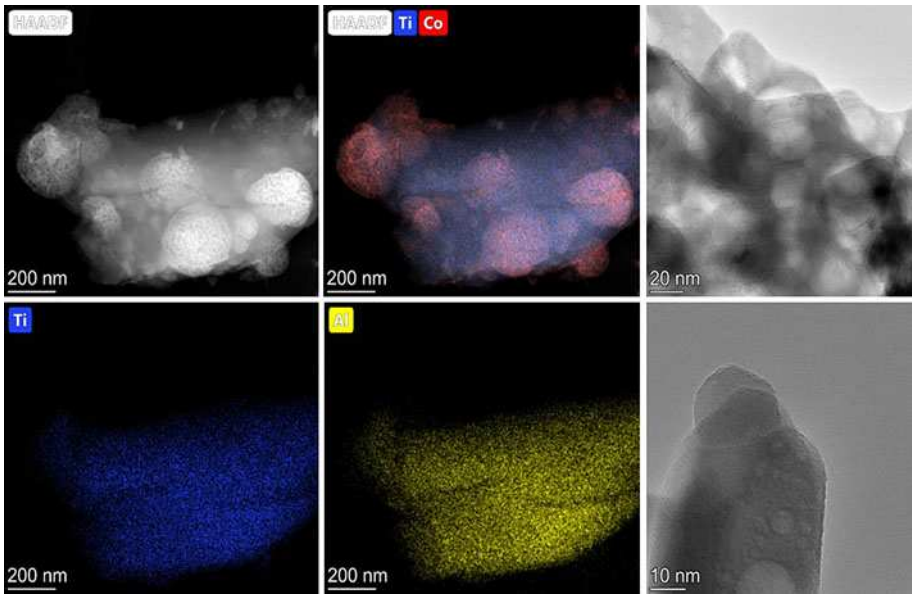

Figure 3. HAADF-STEM images of Co_3O_4/Ti_2AlC catalyst.

temperature.[32,33] Broad and/or multiple peaks can appear at higher temperatures, depending on the CoO–support interactions.

The Co_3O_4/Ti_2AlC reduction profile shows a small reduction peak at 350 °C, overlapping with a second intense peak at 376 °C, and a third at 517 °C. The first peak is attributed to either the reduction of bulk Co_3O_4 (Co_3O_4 particles with a weak interaction with the support), or to the reduction of residual cobalt nitrate.[34] The second and third peaks correspond to the reduction of supported Co_3O_4 to CoO, and CoO to Co, respectively. The Co_3O_4/Al_2O_3 reduction profile is similar to that of Co_3O_4/Ti_2AlC, indicating that both contain Co_3O_4 species with a similar interaction with the support. In contrast, the TPR of Co_3O_4/Al_2O_3 shows a third reduction peak at 790 °C, attributed to the reduction of CoO species with a stronger interaction with the support, that is, the reduction of the spinel $CoAl_2O_4$ phase.[35] Only one intense reduction peak is seen for the Co_3O_4/TiO_2 catalyst, assigned to the overlap of the two-step reduction of Co_3O_4.[36]

Catalyst testing

The catalytic tests were performed in an automated six-flow parallel reactor system, with six quartz tube reactors.[37] 100 mg of catalyst (in the form of pellets) was placed in the reactor. We ran two types of catalytic tests: temperature screening between 450 and 650 °C, and long-term stability tests at 650 °C for 18 h. The reactants ratio ($CO_2/C_4H_{10} = 4:1$), pressure (atmospheric), and total flow rate were kept constant.

Control experiments comparing fresh and calcined samples of Ti_2AlC did not show any conversion (Figure S5), confirming the need for a metal or metal oxide as the active site. In addition, the pre-reduction of the supported catalysts at 650 °C for 1 h did not show any improvement on the catalytic performance compared to the unreduced catalysts (Figure S5). Therefore, we focus on discussing the catalytic tests of the as-prepared materials, without pre-reduction.

The temperature screening tests showed that the Co_3O_4/Ti_2AlC catalyst is active for dry reforming at 450 °C and above (Figure 4). The CO_2 conversion reached 38% at 650 °C. This is a promising result as it shows that the catalyst is active despite the low surface area of the MAX phase support and the larger size of the cobalt oxide particles. The catalyst is highly selective towards CO and H_2 (64 and 35%, respectively), giving only trace amounts of olefins (< 1% of the total mixture). We used a stoichiometric ratio of the reactants (4:1 CO_2/C_4H_{10}), and therefore expected a H_2/CO ratio of 0.6:1. However, the actual H_2/CO ratio ranged between 0.3–0.5 from 550 to 650 °C (Figure S6). This indicates extra production of CO and/or consumption of H_2, possibly caused by reverse water gas shift (RWGS), which is a common side reaction during dry reforming reactions.[38,39]

Encouraged by the activity of this low-surface-area catalyst, we also tested its long-term stability at 650 °C for 18 h (Figure 5). The catalyst converted 24% CO_2 in the beginning of the reaction, and it was stable over time, with only a slight deactivation (2.5% for butane conversion and 1.6% for CO_2 conversion) after 18 h (Figure 5). Moreover, its carbon balance (expressed as C_{out}/C_{in}) was 93%, confirming that very little carbon was deposited on the catalyst.

We then compared the catalytic performance of MAX phase supported cobalt oxide with titania and alumina supported cobalt oxide. Co_3O_4/TiO_2 catalyst gave very low conversion: 12% of butane was converted at the beginning of the reaction, but this quickly decayed to 5% butane conversion. However, this observed conversion corresponds to the thermal cracking of butane to C_2 compounds. Neither CO or H_2 were detected as

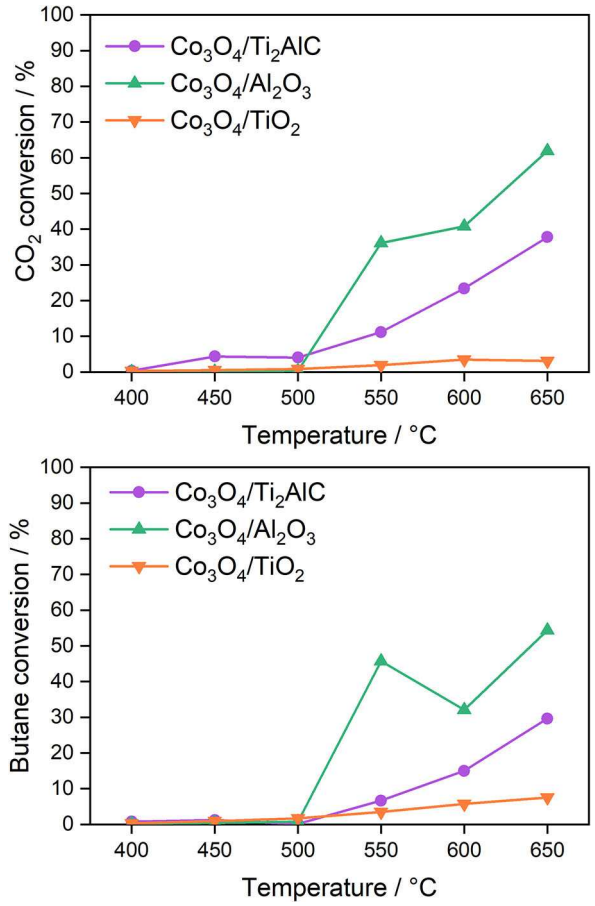

Figure 4. CO_2 and butane conversion during temperature screening of the 5 wt% catalysts. Reaction conditions: 100 mg of catalyst, $CO_2/C_4H_{10}=4:1$, total flow 20 mL·min^{-1}, atmospheric pressure.

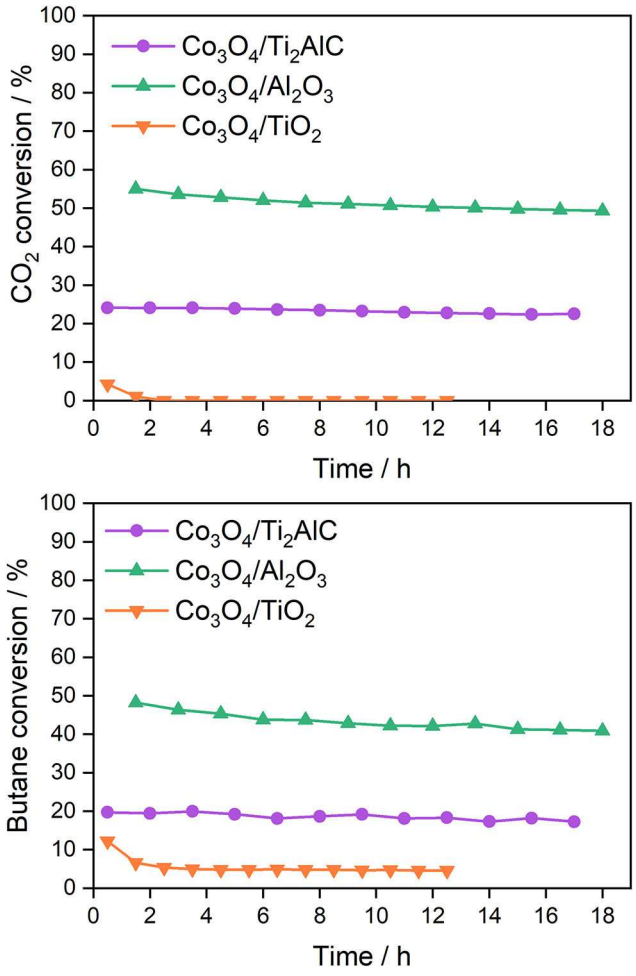

Figure 5. CO_2 and butane conversion during stability test of the 5 wt% catalysts. Reaction conditions: 650 °C, 100 mg of catalyst, $CO_2/C_4H_{10}=4:1$, total flow 20 mL·min^{-1}, atmospheric pressure.

products (Figure S7). HAADF-STEM images of the spent catalyst (Figure S8) show the sintering of cobalt oxide particles compared to the fresh sample, which explains the deactivation of this catalyst.

Co_3O_4/Al_2O_3 showed a higher conversion than cobalt on MAX phase. However, its temperature-screening profile (Figure 4) shows a decrease in conversion at 600 °C compared to the conversion at 550 °C. This is due to the predominance of coking by butane cracking and/or the Boudouard reaction, which leads to a significant amount of deposited carbon (33–22%) that deactivates the catalyst. During the stability test, Co_3O_4/Al_2O_3 deactivates more (7.3% for butane conversion and 5.7% for CO_2 conversion) than the MAX phase catalyst. The carbon balance is only 85%, indicating considerably more carbon deposition (15%) on the catalyst surface (see Figure S7). Thermogravimetric analysis (TGA, Figure S9) of the spent catalyst confirms the deposition of coke during reaction, since there is a mass loss between 300 and 600 °C corresponding to the combustion of soft coke.[40,41] Typically, the rate and extent of coke formation increase with increasing acidity of the catalyst.[42] Since Co_3O_4/Ti_2AlC is significantly less acidic than Co_3O_4/Al_2O_3 [see NH_3 temperature-programmed desorption (TPD) results in Table S2], it can inhibit coke formation more efficiently. We also ran CO_2 chemisorption experiments, but the low porosity and surface area of Ti_2AlC hinders the adsorption of molecules like CO_2, and no useful information was obtained from these experiments.

Dry reforming is a structure-sensitive reaction, where the catalyst particle size affects its performance.[43] Thus, we compared the intrinsic activity of Co_3O_4/Ti_2AlC and Co_3O_4/Al_2O_3 catalysts based on their turnover frequency (TOF, Table 1). The Co_3O_4/Ti_2AlC catalyst shows lower CO uptake, indicating that it contains fewer surface active sites due to its significant larger particle size. Nevertheless, Co_3O_4/Ti_2AlC shows slightly lower

Table 1. CO uptake and TOF values (measured at 12 h of the stability test reaction at 650 °C) of Co_3O_4/Ti_2AlC and Co_3O_4/Al_2O_3.

Catalyst	CO uptake [$\mu mol_{CO}\, g_{catalyst}^{-1}$]	TOF CO_2 [$mol_{converted}$ cobalt $site^{-1}\, min^{-1}$]	TOF butane [$mol_{converted}$ cobalt $site^{-1}\, min^{-1}$]
Co_3O_4/Ti_2AlC	5.4	76.0	14.8
Co_3O_4/Al_2O_3	8.5	104.8	21.2

TOF values, indicating that it is intrinsically less active than Co_3O_4/Al_2O_3.

Additionally, we compared Ti_2AlC MAX phase to commercial TiC and α-Al_2O_3 as cobalt oxide supports. During the temperature screening tests (Figure S10), the Co_3O_4/TiC catalyst (S_{BET} = 28 $m^2 \cdot g^{-1}$) showed significant conversion only at 650 °C. During the stability test at 650 °C (Figure S11), TiC decomposed to rutile TiO_2 and graphite (Figure S12a), clogging the reactor after 2 h under stream. This demonstrates the enhanced stability of Ti_2AlC ternary carbide compared to a traditional carbide under dry reforming conditions. Co_3O_4/α-Al_2O_3 (S_{BET} = 8 $m^2 \cdot g^{-1}$) already showed activity at 450 °C, but the presence of coke clogged the reactor. The XRD pattern of the spent catalyst confirms the formation of graphite oxide (Figure S12b).[44] Similarly to the γ-Al_2O_3-based catalyst, Co_3O_4/α-Al_2O_3 shows strong deactivation during the stability test at 650 °C (Figure S11). Even though it shows higher conversion than Co_3O_4/Ti_2AlC, the carbon balance was only 85–89%, indicating its higher tendency to form coke.

Further insight into the workings of these catalysts was gained from X-ray photoelectron spectroscopy (XPS) studies of pristine and spent catalyst samples. The spectra of the pure Ti_2AlC show the characteristic peaks of the MAX phase structure (Figure 6): the Ti $2p_{3/2}$ spectrum exhibits the Ti–C bond peak at 453.6 eV, and the Al $2p_{3/2}$ spectrum shows the Al–Ti bond peak at 71.6 eV.[45] The presence of oxygen on the surface of the MAX phase is also detected (Ti–O and Al–O peaks), showing that the MAX phase contains an oxide layer on the surface, in agreement with previous observations.[24,45]

During the calcination of the Co_3O_4/Ti_2AlC catalyst, the surface of the MAX phase changes (Figure 6). The absence of characteristic Ti–C and Al–Ti peaks indicates that the surface is partially oxidized during the preparation of the catalyst. The C 1s spectrum affirms these findings (Figure S13). The Ti–C peak that appears at 281.1 eV in the Ti_2AlC sample is not visible after impregnation and calcination. This surface restructuring was observed by Frodelius et al., who studied the oxidation behavior of Ti_2AlC at 500 °C.[46] They showed that at this temperature, Al diffuses out of the crystal lattice and migrates to the surface. Oxygen from the atmosphere then reacts with the Al, forming amorphous Al_2O_3. In parallel, the Al vacancies enable oxygen-inward diffusion, which promotes the formation of TiO_xC_y. The transport of Al to the surface is much faster than that of Ti atoms. This is because the Ti–Al bond is of metallic character, whereas the transport of Ti atoms is limited by the Ti–C covalent bond.[47] Surface TiO_xC_y and Al–TiO_xC_y species were detected for the Co_3O_4/Ti_2AlC catalyst (Figure 6).

The Co 2p spectrum is characterized by the doublet of two spin-orbit components, Co $2p_{3/2}$ and Co $2p_{1/2}$. Literature reported that Co_3O_4 shows its main peak at 779.6 eV (Co $2p_{3/2}$), with different satellite signals originating from Co^{3+} and Co^{2+} species.[48] Figure 7 shows that Co_3O_4 species have different binding energies depending on the support. The main peak appears at 779.4, 780, and 782 eV for Co_3O_4/Ti_2AlC, Co_3O_4/TiO_2, and Co_3O_4/Al_2O_3, respectively. The Co 2p spectrum of Co_3O_4/Ti_2AlC catalyst shows the main Co 2p peak at lower binding energy compared to the other catalysts. Moreover, it has an additional contribution at 777.5 eV, showing the metallic character of the surface of this sample, induced by the Ti_2AlC

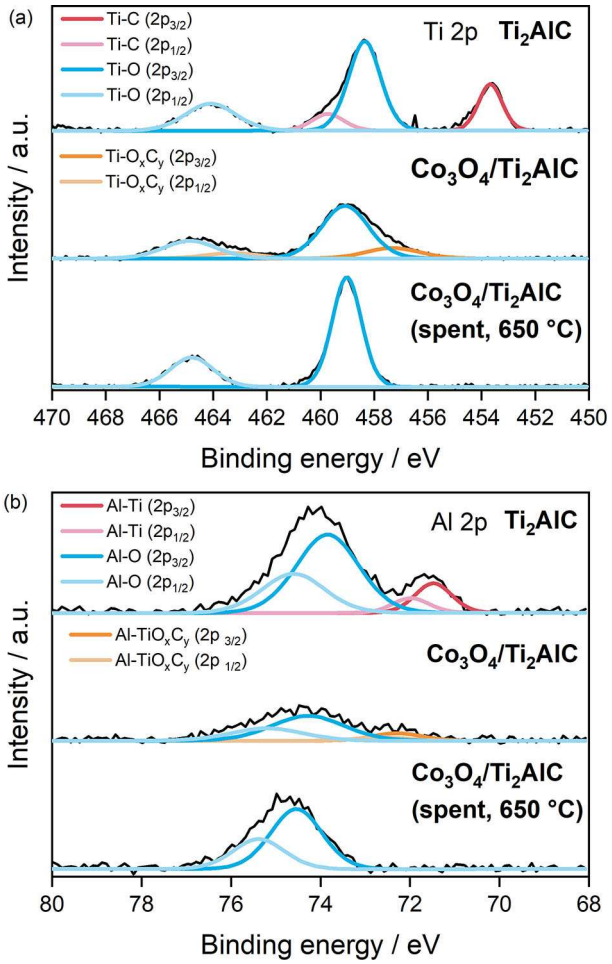

Figure 6. XPS spectra of the Ti_2AlC MAX phase support, fresh Co_3O_4/Ti_2AlC catalyst and Co_3O_4/Ti_2AlC after stability test (spent, 650 °C). a) Ti 2p, b) Al 2p.

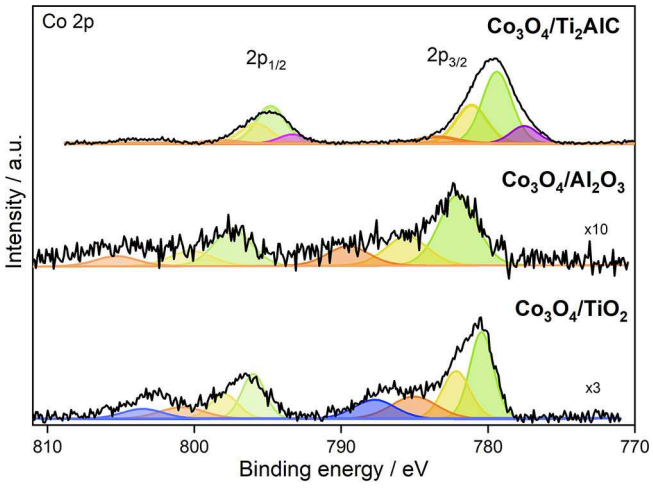

Figure 7. Co 2p XPS spectra of the fresh Co_3O_4/Ti_2AlC, Co_3O_4/Al_2O_3, and Co_3O_4/TiO_2 catalysts.

support. In addition, the intensity ratio between cobalt and support particles (I_{Co}/I_{Al} or I_{Co}/I_{Ti}) is the largest among the three catalysts (see Table S3). As all three catalysts have the same cobalt oxide loading, the smaller surface area of the MAX phase results in a poor particle dispersion.

Following the stability test at 650 °C, the Co 2p spectra of Co_3O_4/Ti_2AlC (Figure S14) shift to higher binding energies (for instance, the main $Co\,2p_{3/2}$ peak shifts to 781.1 eV). This indicates that the Ti_2AlC surface oxidizes under reaction conditions. A thicker layer of oxide between the Co_3O_4 and the bulk Ti_2AlC reduces the metallic character of the sample, shifting the Co 2p spectrum to higher binding energies. In addition, the Ti 2p and Al 2p spectra show lines corresponding to the Ti–O and Al–O bonds, with no contributions of TiO_xC_y and Al–TiO_xC_y (Figure 6). This indicates the total oxidation of the Ti_2AlC surface during the reaction, probably due to the prolonged exposure of the catalyst to CO_2 at 650 °C. Studies on the oxidation of Ti_2AlC at 1200 °C showed that a continuous inner layer of α-Al_2O_3 and a discontinuous outer layer of TiO_2 (rutile) form on the surface.[47] These layers are responsible for the "high thermal stability" of Ti_2AlC, because they protect the rest of the material that is not oxidized.[18] The XRD pattern of the spent sample (Figure S15) has the characteristic peaks of the MAX phase, indicating that the bulk of the Ti_2AlC remains stable.

As the Ti_2AlC surface composition changes during reaction, the supported Co_3O_4 is also affected. HAADF-STEM images of the spent catalyst show a change in morphology and absence of voids (Figure S16). Co_3O_4 particles migrate over the support under reaction, resulting in a very heterogeneous surface in terms of size and morphology. Large and small Co_3O_4 particles are observed, but their irregular shape makes it difficult to determine the particle size distribution. Carbon nanotubes are also observed, covering some cobalt oxide particles (Figure S17). These structural changes did not significantly affect the number of active sites, as its activity remained stable over time (Figure 5). Figure 8 summarizes the compositional and structural changes on the surface of the Co_3O_4/Ti_2AlC catalyst during calcination and reaction.

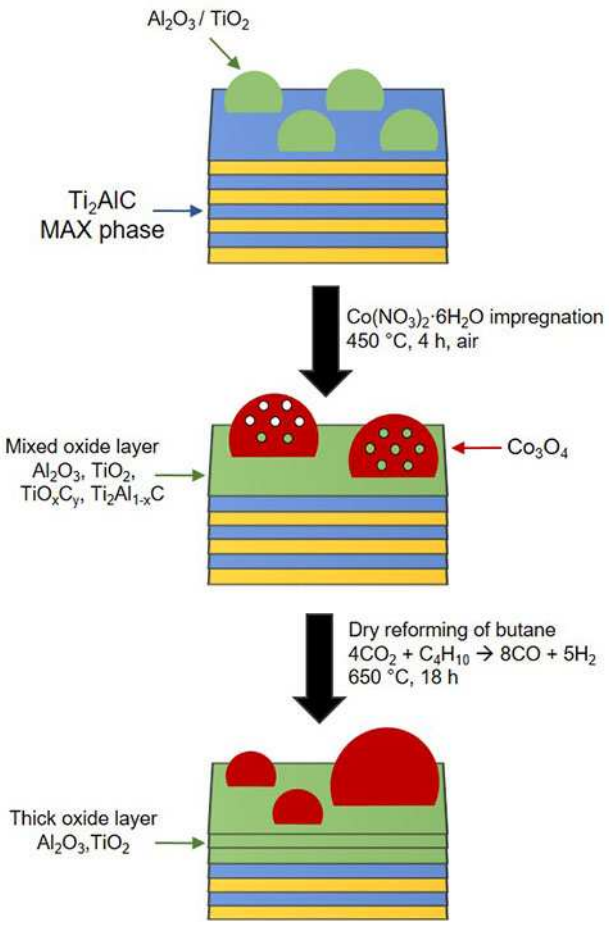

Figure 8. Structural changes on the Ti_2AlC-based catalyst after being exposed to impregnation and butane dry reforming reaction conditions.

Conclusions

Overall, this study shows the importance of the support in dry reforming catalysis. MAX phases are promising supports, as they show reasonable activity and high stability. The low surface area of Ti_2AlC influences the size and morphology of Co_3O_4, forming large hollow Co_3O_4 particles. A charge transfer effect is observed in the shift of the Co 2p spectrum to lower binding energies, probably caused by the conductive and metallic properties of the support. While this catalyst is less active than Co_3O_4/γ-Al_2O_3, its conversion is remarkable given the difference in particle size and surface area. In addition, it is less prone to coking, making the catalyst more stable. This is an advantage compared to using acidic materials such as γ-alumina as the support, where their acidic properties favor the formation of undesirable coke. Furthermore, compared to titania and titanium carbide, the MAX phase support is more stable. It does not deactivate by sintering or thermal decomposition. Thus, we conclude that MAX phases are promising supports for dry reforming reactions, thanks to their thermal stability and their electronic and acid-base properties. Nevertheless, the intrinsic activity of MAX phases is limited by the low number of active sites on the surface. Increasing the number of cobalt oxide active sites, which can be done by decreasing the particle size, would increase the performance of this catalyst. We hope that this exciting first account of using MAX phases as catalyst supports in CO_2 conversion reactions may encourage more researchers to apply these fascinating materials in catalysis.

Experimental Section

Materials and instrumentation: Powder XRD patterns were recorded on a MiniFlex II diffractometer using CuK_α radiation. The X-ray tube was operated at 30 kV and 15 mA. Measurements were recorded at an angle (2θ) range of 5–90° with a turning speed of $2.5^\circ \cdot min^{-1}$. N_2 adsorption-desorption isotherms were measured on a Thermo Scientific Surfer instrument at 77 K. The samples were pre-treated in vacuum for 12 h at 200 °C. XPS was performed using

a K-Alpha spectrometer from Thermo-Scientific. Al–K radiation (1486.6 eV), monochromatized by a twin crystal monochromator was used. This resulted in a focused X-ray spot (400 μm diameter), at 3 mA × 12 kV when charge compensation was achieved with the system flood gun, which provides low energy electrons and low energy argon ions from a single source. The alpha hemispherical analyzer was operated in constant energy mode with survey scan pass energies of 200 eV to measure the whole energy band, and 50 eV in a narrow scan to selectively measure particular elements. The binding energies (BE) were referenced to the C 1s line at 284.6 eV, with an accuracy of ±0.2 eV. The intensity estimation was done by calculating each peak integral, subtracting the S-shaped background, and fitting the experimental curve to a combination of a Lorentzian (30%) and Gaussian (70%) lines.[49]

TEM characterization of the samples was performed using a double Cs aberration-corrected FEI Titan^3 Themis 60–300 microscope. This equipment was operated at 200 kV and it is equipped with a monochromator, a X-FEG gun and a high efficiency XEDS Chem-iSTEM, which consists of 4-windowless SDD detectors. HR-STEM imaging was performed using a HAADF detector with a camera length of 11.5 cm. The HAADF-STEM technique is sensitive to the atomic number of the elements and it makes possible to distinguish small nanoparticles supported on light supports. Energy-dispersive X-ray spectroscopy mappings were performed using a beam current of 200 pA and a dwell time per pixel of 128 μs. To improve the visual quality of the elemental maps, these were filtered using a Gaussian blur of 0.8 using Velox software. TPR measurements were performed using a TPDRO Series 1100 from Thermo Scientific. 25 mg of catalyst was placed on a quartz wool plug in a tubular quartz reactor with an inner diameter of 4 mm. Each sample was heated from room temperature to 1000 °C (heating rate 5 °C·min^{-1}) under a flow of 5% hydrogen in nitrogen mixture (20 mL·min^{-1}). The amount of hydrogen consumed by the sample was detected by a thermal conductivity detector (TCD). TGA was performed using a NETZSCH Jupiter® STA 449F3 instrument. The measurements were done under air (20 mL·min^{-1}, O_2/N_2 mixture) between 30 and 1000 °C at a heating rate of 5 °C·min^{-1}.

NH_3 adsorption and subsequent TPD were performed in a Hiden CATLABPCS combined micro reactor and mass spectrometer (MS) system as reported in the literature.[50] Experiments were performed according to the following steps. Firstly, stabilization of a flow of pure He (30 mL·min^{-1}) at 50 °C for 25 min in order to check the sensitivity factor of He. Secondly, adsorption of NH_3 at 150 °C for 1.5 h from a 95:5 He/NH_3 flow (25 mL·min^{-1}) mixed with a flow of pure He (5 mL·min^{-1}). Then, flushing at 100 °C under pure He (30 mL·min^{-1}) for 2.5 h in order to eliminate the physisorbed NH_3. Finally, TPD from 100 to 650 °C (10 °C·min^{-1} under 30 mL·min^{-1} of pure He) in order to desorb chemisorbed NH_3. We also performed CO chemisorption analysis, using a Micromeritics Pulses Chemisorb 2705 apparatus. Before the analysis, the samples were pretreated under helium gas flow of 80 mL·min^{-1} at 350 °C for 3 h. For the analysis, CO pulses of known volume were consecutively injected into the He stream flowing through the catalyst (300 mg) at 35 °C. After each injection, the apparatus gave a peak area (A_p) corresponding to the non-adsorbed CO. When the surface was saturated, the peak area reached the maximum (A_{max}), which corresponds to the volume of the CO injected (V_{CO}). To correlate the moles of non-adsorbed CO with the peak area, a calibration factor was calculated.

Procedure for catalyst synthesis: Samples containing 5 wt% of cobalt metal were prepared by wet impregnation using Co $(NO_3)_2 \cdot 6H_2O$ (99%, Acros Organics) as metal oxide precursor and Ti_2AlC, TiO_2 (Hombicat), TiC (VWR International B.V.), γ-Al_2O_3 (CK-300, Ketjen), and α-Al_2O_3 (Alfa Aesar) as supports. 0.53 g of Co $(NO_3)_2 \cdot 6H_2O$ dissolved in 10 mL of water was poured into a slurry containing 2 g of support and 10 mL of water (total solution/solid ratio of 10 mL·g^{-1}). The resulting slurry was stirred under heating at 65 °C for 24 h, until the water was completely evaporated. After impregnation, the catalysts were dried under air at 120 °C for 2 h and then calcined under air at 450 °C for 4 h (heating rate 4 °C·min^{-1}), except for the TiC-based catalyst that was heated under N_2 (150 ml·min^{-1}) up to 300 °C. Ti_2AlC was prepared by mixing elemental powders of Ti, Al, and TiC, and heating to 1350 °C under a pressure of up to 50 MPa, following a published procedure.[18]

Procedure for catalytic testing: The catalysts were tested in the DRB reaction in an automated six-flow parallel reactor system. Typically, 100 mg of catalyst was placed in the reactor in form of pellets (1–0.71 mm pellet size). A stoichiometric ratio of reactants ($CO_2/C_4H_{10} = 4:1$) and atmospheric pressure were used for all tests. The feed gas was diluted with 80% of Ar and a total flow rate of 20 mL·min^{-1} was passed through the reactors. We ran two types of catalytic tests: temperature screening between 450 and 650 °C, and stability test at 650 °C. The reactants and products were analyzed with a GC (Interscience microGC, with flame ionization detector and TCD).

Conversion, selectivity, and TOF were calculated using Equations (1)–(3):

$$\text{Conversion reactant } [\%] = \frac{[\text{reactant}]_{in} - [\text{reactant}]_{out}}{[\text{reactant}]_{in}} \cdot 100 \quad (1)$$

$$\text{Selectivity product A } [\%] = \frac{[\text{product A}]_{out}}{\Sigma[\text{products}]_{out}} \cdot 100 \quad (2)$$

$$\text{TOF reactant } [\text{mol}_{\text{reactant converted}} \cdot \text{site}^{-1} \cdot \text{min}^{-1}] = \frac{\text{flow reactant} \cdot \text{conversion reactant}}{\text{CO uptake} \cdot \text{weight catalyst}} \quad (3)$$

Acknowledgements

We thank the Netherlands Organization for Scientific Research (NWO) for the grant "Developing novel catalytic materials for converting CO_2, methane and ethane to high-value chemicals in a hybrid plasma-catalytic reactor" (China.15.119). We also acknowledge financial support by MINECO (Spain) through projects MAT2017-86992-R and MAT2016-80285-P.

Conflict of Interest

The authors declare no conflict of interest.

Keywords: butane dry reforming · cobalt oxide · CO_2 conversion · MAX phases · Ti_2AlC support

[1] D. Lüthi, M. Le Floch, B. Bereiter, T. Blunier, J. M. Barnola, U. Siegenthaler, D. Raynaud, J. Jouzel, H. Fischer, K. Kawamura, T. F. Stocker, *Nature* **2008**, *453*, 379–382.
[2] M. Ronda-Lloret, G. Rothenberg, N. R. Shiju, *ChemSusChem* **2019**, *12*, 3896–3914.
[3] S. C. Peter, *ACS Energy Lett.* **2018**, *3*, 1557–1561.

[4] E. S. Gnanakumar, N. Chandran, I. V. Kozhevnikov, A. Grau-Atienza, E. V. Ramos Fernández, A. Sepulveda-Escribano, N. R. Shiju, *Chem. Eng. Sci.* **2019**, *194*, 2–9.
[5] E. Devid, D. Zhang, D. Wang, M. Ronda-Lloret, Q. Huang, G. Rothenberg, N. R. Shiju, A. W. Kleyn, *Energy Technol.* **2020**, *8*, 1900886.
[6] Y. T. Shah, T. H. Gardner, *Catal. Rev.* **2017**, *56*, 476–536.
[7] Y. T. Shah, T. H. Gardner, *Catal. Rev.* **2014**, *56*, 476–536.
[8] J. Sarkar, S. Bhattacharyya, *Arch. Thermodyn.* **2012**, *33*, 23–40.
[9] C. M. Freeman, G. J. Moridis, T. A. Blasingame, *Transp. Porous Media* **2011**, *90*, 253–268.
[10] B. Yao, W. Ma, S. Gonzalez-Cortes, T. Xiao, P. P. Edwards, *Greenh. Gas Sci. Technol.* **2017**, *7*, 942–957.
[11] E. Gomez, B. Yan, S. Kattel, J. G. Chen, *Nat. Rev. Chem.* **2019**, *3*, 638–649.
[12] E. Gomez, Z. Xie, J. G. Chen, *AIChE J.* **2019**, *65*, 16670.
[13] M. D. Porosoff, M. N. Z. Myint, S. Kattel, Z. Xie, E. Gomez, P. Liu, J. G. Chen, *Angew. Chem. Int. Ed.* **2015**, *54*, 15501–15505; *Angew. Chem.* **2015**, *127*, 15721–15725.
[14] T. W. Hansen, A. T. Delariva, S. R. Challa, A. K. Datye, *Acc. Chem. Res.* **2014**, *46*, 1720–1730.
[15] M.-S. Fan, A. Z. Abdullah, S. Bhatia, *ChemCatChem* **2009**, *1*, 192–208.
[16] J. Beckers, G. Rothenberg, *Dalton Trans.* **2008**, 6573–6578.
[17] M. Barsoum, T. El-Raghy, *Am. Sci.* **2001**, *89*, 334–343.
[18] L. Boatemaa, M. Bosch, A. S. Farle, G. P. Bei, S. van der Zwaag, W. G. Sloof, *J. Am. Ceram. Soc.* **2018**, *101*, 5684–5693.
[19] Y. Medkour, A. Roumili, D. Maouche, L. Louail, *Advances in Science and Technology of $M_{n+1}A_Xn$ Phases*, Woodhead Publishing Limited, **2012**, pp. 159–175.
[20] X. H. Wang, Y. C. Zhou, *Corros. Sci.* **2003**, *45*, 891–907.
[21] W. G. Sloof, R. Pei, S. A. McDonald, J. L. Fife, L. Shen, L. Boatemaa, A. S. Farle, K. Yan, X. Zhang, S. Van Der Zwaag, P. D. Lee, P. J. Whiters, *Sci. Rep.* **2016**, *6*, 23040.
[22] G. W. Bentzel, M. Sokol, J. Griggs, A. Lang, M. W. Barsoum, *J. Alloys Compd.* **2019**, *771*, 1103–1110.
[23] J. Xiao, C. Wang, T. Yang, S. Kong, J. Xue, Y. Wang, *Nucl. Instrum. Methods Phys. Res. Sect. B* **2013**, *304*, 27–31.
[24] W. H. K. Ng, E. S. Gnanakumar, E. Batyrev, S. K. Sharma, P. K. Pujari, H. F. Greer, W. Zhou, R. Sakidja, G. Rothenberg, M. W. Barsoum, N. R. Shiju, *Angew. Chem. Int. Ed.* **2018**, *57*, 1485–1490; *Angew. Chem.* **2018**, *130*, 1501–1506.
[25] K. N. Papageridis, G. Siakavelas, N. D. Charisiou, D. G. Avraam, L. Tzounis, K. Kousi, M. A. Goula, *Fuel Process. Technol.* **2016**, *152*, 156–175.
[26] B. Jongsomjit, *J. Catal.* **2001**, *204*, 98–109.
[27] X. Liu, M. Khan, W. Liu, W. Xiang, M. Guan, P. Jiang, W. Cao, *Ceram. Int.* **2015**, *41*, 3075–3080.
[28] S. W. Chee, S. F. Tan, Z. Baraissov, M. Bosman, U. Mirsaidov, *Nat. Commun.* **2017**, *8*, 1224.
[29] D. H. Ha, L. M. Moreau, S. Honrao, R. G. Hennig, R. D. Robinson, *J. Phys. Chem. C* **2013**, *117*, 14303–14312.
[30] D. Wang, Y. Yu, H. He, J. Wang, W. Zhou, H. D. Abruña, *ACS Nano* **2015**, *9*, 1775–1781.
[31] A. Shahzad, M. Nawaz, M. Moztahida, K. Tahir, J. Kim, Y. Lim, B. Kim, J. Jang, D. S. Lee, *ACS Appl. Mater. Interfaces* **2019**, *11*, 19156–19166.
[32] L. Borko, *Top. Catal.* **2002**, *20*, 129–139.
[33] O. O. James, M. Sudip, *J. Pet. Technol. Altern. Fuels* **2016**, *7*, 9824F0256972..
[34] Y. Ji, Z. Zhao, A. Duan, G. Jiang, J. Liu, *J. Phys. Chem. C* **2009**, *113*, 7186–7199.
[35] J. L. Rogers, M. C. Mangarella, A. D. D'Amico, J. R. Gallagher, M. R. Dutzer, E. Stavitski, J. T. Miller, C. Sievers, *ACS Catal.* **2016**, *6*, 5873–5886.
[36] B. Jongsomjit, J. Panpranot, J. G. Goodwin, *J. Catal.* **2001**, *204*, 98–109.
[37] J. H. Blank, J. Beckers, P. F. Collignon, F. Clerc, G. Rothenberg, *Chem. Eur. J.* **2007**, *13*, 5121–5128.
[38] I. G. Osojnik Črnivec, P. Djinović, B. Erjavec, A. Pintar, *Chem. Eng. J.* **2012**, *207–208*, 299–307.
[39] M. S. Aw, I. G. Osojnik Črnivec, P. Djinović, A. Pintar, *Int. J. Hydrogen Energy* **2014**, *39*, 12636–12647.
[40] W.-W. Liu, A. Aziz, S.-P. Chai, A. R. Mohamed, C.-T. Tye, *New Carbon Mater.* **2011**, *26*, 255–261.
[41] W. W. Liu, S. P. Chai, A. R. Mohamed, U. Hashim, *J. Ind. Eng. Chem.* **2014**, *20*, 1171–1185.
[42] C. H. Bartholomew, *Appl. Catal. A* **2001**, *212*, 17–60.
[43] C. Vogt, J. Kranenborg, M. Monai, B. M. Weckhuysen, *ACS Catal.* **2020**, *10*, 1428–1438.
[44] H. C. Lee, W. W. Liu, S. P. Chai, A. R. Mohamed, A. Aziz, C. S. Khe, N. M. S. Hidayah, U. Hashim, *RSC Adv.* **2017**, *7*, 15644–15693.
[45] K. Chen, N. Qiu, Q. Deng, M. H. Kang, H. Yang, J. U. Baek, Y. H. Koh, S. Du, Q. Huang, H. E. Kim, *ACS Biomater. Sci. Eng.* **2017**, *3*, 2293–2301.
[46] J. Frodelius, J. Lu, J. Jensen, D. Paul, L. Hultman, P. Eklund, *J. Eur. Ceram. Soc.* **2013**, *33*, 375–382.
[47] G. M. Song, V. Schnabel, C. Kwakernaak, S. Van Der Zwaag, J. M. Schneider, W. G. Sloof, *Mater. High Temp.* **2012**, *29*, 205–209.
[48] M. C. Biesinger, B. P. Payne, A. P. Grosvenor, L. W. M. Lau, A. R. Gerson, R. S. C. Smart, *Appl. Surf. Sci.* **2011**, *257*, 2717–2730.
[49] D. A. Shirley, *Phys. Rev. B* **1972**, *5*, 4709–4714.
[50] V. S. Marakatti, S. Marappa, E. M. Gaigneaux, *New J. Chem.* **2019**, *43*, 7733–7742.

Manuscript received: July 8, 2020
Revised manuscript received: August 27, 2020
Version of record online: September 18, 2020